International Journal of Nanoelectronics and Materials
IJNeaM
ISSN 198-5761 | E-ISSN 2232-1535

Structural, Morphological, and Electrochemical Properties of MXene/MoS_2-based Supercapacitor

Muhammad Akmal Kosnan[a], Mohd Asyadi Azam[a,b,*], Rose Farahiyan Munawar[a], Alicja Klimkowicz[b] and Akito Takasaki[b]

[a]*Fakulti Teknologi dan Kejuruteraan Industri dan Pembuatan, Universiti Teknikal Malaysia Melaka, Hang Tuah Jaya, 76100 Durian Tunggal, Melaka, Malaysia.*
[b]*Department of Engineering Science and Mechanics, College of Engineering, Shibaura Institute of Technology, 3-7-5 Toyosu, Koto-Ku, Tokyo 135-8548, Japan.*
**Corresponding author. Tel.: +606-270 2571; Fax: +606-270 1047; e-mail: asyadi@utem.edu.my*

ABSTRACT

Two-dimensional (2D) materials, inclusive of molybdenum disulfide (MoS_2), are auspicious due to their structure providing absorption sites and shorter diffusion paths. However, their sheet restacking affects the functional properties, resulting in the device's low efficiency. A strategy is proposed to combine MoS_2 with MXene material. X-ray Diffraction data revealed peaks at d-spacings of 6.07, 2.72, 2.49, 2.27, 1.82, and 1.53 Å. X-ray photoelectron spectroscopy shows prominent peaks for C 1s and Ti 2p, with no signal for Al detected in the pristine Ti_3C_2 MXene. This indicates successful etching of the Al layer. Electron Microscopes were used to confirm the samples' morphology and showed that the hybrid sample has a layered flake-like structure with a small sphere attached to the surface. While the HR-TEM confirmed the layered structure of Ti_3C_2 after exfoliation from Ti_3AlC_2, consistent with prior studies. Prior, the electrochemical performances of the MXene/MoS_2 supercapacitor in 6M KOH aqueous electrolyte were examined through cyclic voltammetry and galvanostatic charge–discharge. The highest specific capacitance reached was 139.71 Fg^{-1}, attributed to heterostructures of an equally distributed MoS_2 and MXene. Furthermore, the device retained about 83% of its initial capacitance after 10,000 cycles of cyclic stability testing. The results demonstrated that the MXene material improved the capacitive performance of MoS_2, and conversely. Further enhancements can be expected as a result of a major omission in electrode synthesis, particularly the importance of delamination in MXene preparation.

Keywords: *MXene, MoS_2, hybrid electrode compositions, characterization, supercapacitor, specific capacitance, electrochemical performance*

1. INTRODUCTION

A supercapacitor (SC) is an electrochemical energy storage system that has great power density and specific capacitance. Unlike normal capacitors that store energy electrostatically, different SCs rely on various electrical charge storage mechanisms such as electric double-layer capacitance (EDLC), pseudocapacitance, or hybrid mechanisms to store and release energy [1], [2]. Supercapacitors are known for their ability to deliver high power density, but advancements in materials and design have also led to improvements in energy density, allowing supercapacitors to store more energy per unit mass or volume [3]. They are known for their ability to withstand a significantly higher number of charge-discharge cycles compared to normal batteries. This is due to the electrostatic charge storage mechanism in supercapacitors, which involves the physical movement of ions within the electrolyte and between the electrodes, rather than the chemical reactions involved in batteries [4], [5]. Electricity plays a major role in our daily lives, but it is not easy to store it quickly. So, the focus will be on proficient energy storage for effective consumption or utilization in any needed field [6]. Nowadays, industry 4.0 demands portable grid-less energy devices, including supercapacitors. As the reports stated, a supercapacitor is a great energy storage device, that is reusable over many cycles [7]. However, for future development, supercapacitors require an enhancement in the amount of specific capacitance and an even better rate for cycling stability. The supercapacitor electrode material plays a vital part in both requirements to increase the device performance [8], [9].

2D materials are of great interest nowadays. For example, molybdenum disulphide (MoS_2) is a bright material because of its structure, providing adsorption sites and short ion diffusion paths. However, restacking among MoS_2 sheets showed a reduction of their functional properties and resulted in low efficiency of the device [10-12]. In this study, a strategy to tackle this problem is to design novel heterostructures composed of MoS_2 with MXene as a hybrid material [13]. MXene materials are two-dimensional compounds made up of transition metals, carbides, and nitrides that have shown great promise for usage in supercapacitor applications [14]. MXenes are typically synthesised by selectively eliminating the A-group individual, which refers to the elements in the first column of the periodic table, also called alkali metals, from MAX phases. While MAX phases are layered ternary compounds containing carbides and nitrides. This technique yields MXene materials with a distinct layered structure, high specific surface area, outstanding electrical

conductivity, and remarkable mechanical flexibility, which is desirable from the application viewpoint [15]. The appeal of MXene materials for supercapacitor applications stems from their distinct physicochemical properties, which facilitates electrochemical reactions, efficient electrical conductivity, mechanical flexibility, which makes them suitable for flexible and wearable supercapacitor devices, and hydrophilic nature, which allows for easy dispersibility in water and other solvents [16]. MXene materials store electric charge using a novel mechanism that involves electrochemical ion adsorption on their surfaces and subsequent charge transfer. Recent research has mostly focused on creating composite materials for supercapacitor electrodes that incorporate MXenes, as well as carbon nanomaterials, metal oxides, and conductive polymers. For example, Ti_3C_2Tx MXene, a representative member of the developing 2D MXene family, has demonstrated remarkable promise as a supercapacitor electrode material [17]. Comprehensive evaluations of latest advances in Ti_3C_2Tx-based supercapacitor electrodes have underlined the critical role of Ti_3C_2Tx MXene in obtaining exceptional electrochemical performance and improving our understanding of the underlying mechanisms.

2D MXene has good electrical conductivity, and it can host many different cations between its layers [18]. These special properties have attracted attention from various fields. MXene-based materials, such as Titanium Carbide (Ti_3C_2), showed varied chemical properties and structures, offering a competitive performance. However, even though stacking on MXene sheets showed good results, surface oxidation remains a challenge. Hence, the creation of hybrid material is suggested as a solution to compensate for the disadvantage of individual materials and possibly improve properties due to a synergic effect. In this study, the prime objective is to combine Ti_3C_2 MXene and MoS_2 through a straightforward hydrothermal synthesis method, followed by the establishment of a relationship between the structural attributes of MXene/MoS_2 and their performance as supercapacitors. This correlation was investigated through analytical techniques, including FESEM, TEM, XPS, and XRD. The focus of this study is not an exhaustive optimization of the synthesis procedure but rather an exploration of the synergic effect of the composite material. The principal aim was to introduce specific enhancements that were strategically crafted to build upon existing knowledge and address identified limitations without undertaking a complete overhaul of the synthesis process.

2. MATERIALS AND METHODS

2.1. Preparation of Ti_3C_2 MXene and MoS_2

To prepare MXene Ti_3C_2, the MAX phase powders, which in this case is titanium aluminum carbide (Ti_3AlC_2), were slowly submerged in a 40% HF solution, and then was constantly stirred for 24 h at room temperature [19]. Then the resultant was washed many times over with deionized water and centrifuged at 3500 rpm for 5 min until the pH value exceeded 6.0. This process was conducted to remove the aluminum. The final resultant was then dried in the vacuum oven at 50 °C for 12 h.

For MoS_2 preparation, thiourea and ammonium molybdate tetrahydrate, $(NH_4)_6Mo_7O_{24}{\cdot}4H_2O$, were solvate in deionized water and stirred vigorously to obtain a homogeneous solution [20]. Then, the mixture was transferred to a Teflon-lined stainless-steel autoclave. The precursor was heated to 210 °C for 40 min and kept for 18 h. Then, the reaction system was naturally cooled to room temperature.

2.2. Preparation of MoS_2/Ti_3C_2 MXene Hybrid Electrode

As-prepared MoS_2 powder was mixed with 0.13 g Ti_3C_2 MXene in the N-methylpyrrolidone (NMP) solution and constantly stirred. The homogeneous resultant was transferred into a Teflon-lined stainless-steel autoclave (28 mL capacity). After that, the experimental procedure is the same to synthesize MoS_2 including drying. The mass of as-synthesized MoS_2/Ti_3C_2 MXene powder was about 0.63g.

A variety of pre-prepared chemicals were readied in advance, including polyvinylidene fluoride (PVDF) binder, acetylene black conductive agent, NMP, and potassium hydroxide (KOH) electrolyte. The slurry was fabricated using a fixed weight ratio set at 80:10:10, allocating 80% to the active material, 10% to the binder, and 10% to the conducting additive. When the active material used was MXene/MoS_2, the individual materials were mixed in equal proportions, as prior research has determined it to be the most optimal ratio. Table 1 below presents the weight ratios for the materials used to create the electrode slurry.

Table 1 Weight composition of MXene/MoS_2 before slurry preparation

Sample	Weight (mg)	Weight composition (%)
MXene powder	2.72	40
MoS_2 powder	2.72	40
PVDF	0.68	10
Acetylene Black	0.68	10

Once all the samples were prepared, they were mixed and agitated in NMP solvent for a minimum of 5 h to ensure the slurry was well dispersed. The final slurry was achieved after continuous stirring for 2–3 h. Using a conventional slurry coating technique, the slurry was applied onto nickel foam, which served as the current collector. Subsequently, the electrodes were allowed to dry. Additionally, material characterization was done using pristine MXene or MoS_2 or the hybrid and sometimes without conducting additive or acetylene black.

2.3. Materials Characterization (XRD, XPS, FESEM, HR-TEM)

X-ray diffraction (XRD; Rigaku MiniFlex) measurement was carried out by using an X-ray beam with a wavelength of 1.5406 Å. The diffraction angle, denoted as 2θ, was adjusted from 5º to 90º. XRD is a suitable technique for assessing the crystallinity of the MXene/MoS_2 hybrid material. The XRD database employed in this research is the XPERT-PRO. In this investigation, we aim to evaluate the crystallinity of pristine MoS_2 and the MXene/MoS_2 hybrid electrode. An X-ray photoelectron spectroscopy (XPS) machine (Kratos AXIS Ultra DLD) was employed to assess the surface chemical characteristics of Ti_3C_2 MXene.

Morphological analyses were done to delve into the intricate details of material surfaces and internal structures and link them with the properties, functionalities, and prospective applications of the studied materials. The field emission scanning electron microscope (FESEM; JEOL JSM-7600F) was used for general observation. The micro-nano sheet/layers analysis was done by a high-resolution transmission electron microscope (HRTEM; JEOL JEM 2100).

2.4. Coin Cell-Type Supercapacitor Fabrication and Electrochemical Performance Evaluation

The fabricated electrodes were assembled in a coin cell to produce a symmetric supercapacitor. 6M of KOH solution was selected as the electrolyte and polypropylene (PP) as the separator. The machine used to perform cyclic voltammetry (CV) and galvanostatic charge–discharge (GCD) measurements was WonAtech WMPG1000. Electrode loading or average active mass per electrode for this work was 6.20 mg.

For cyclic voltammetry (CV) testing, the scan rates were 1, 10, 50, 100, and 250 mVs^{-1} at 0.0 to 1.0 V potential window. The achieved CV curves are then discussed and used to calculate the specific gravimetric capacitance (Csp) value. The equation to calculate the Csp is shown below.

$$C_{sp1} = \frac{A}{mR(V_2 - V_1)} \quad (1)$$

Where (V_2-V_1) = potential window, m = average active mass per electrode, R = scan rates, and A = area under the curve.

For galvanostatic charge–discharge (GCD) testing, the current applied was set at 1.0, 3.0, 6.0, 9.0, and 15.0 mA from a 0.0–1.0 V potential window, which gave a current density of 0.15, 0.48. 0.96, 1.61, and 2.42 Ag^{-1}, respectively. From the GCD results, the equation to calculate specific gravimetric capacitance (C_{sp}) is shown below.

$$Specific\ Capacitance\ , C_{sp2} = \frac{I \times \Delta t}{m \times \Delta V} = \frac{I_m(\Delta t)}{\Delta V} \quad (2)$$

where I = current applied, m = average active mass of electrode, Δt = time difference, I_m = current densities, and ΔV = voltage difference.

The cyclic stability of the MXene/MoS_2-based supercapacitor was evaluated by GCD at a relatively high current density of 2.42 Ag^{-1}. To confirm the MXene/MoS_2-resilience long-term cycle life in the supercapacitor application, capacity retention is crucial.

Both techniques provide information on the capacitance of the electrode material. While CV is a relatively quick technique, making it suitable for initial assessments and screening of electrochemical properties, GCD can provide insights into the stability and performance of your device over longer periods, as it simulates the conditions the device would face during practical use. In this study, the C_{sp} obtained from CV is employed to assess the performance of the devices.

3. RESULTS AND DISCUSSION

3.1. Structural Properties Detected During XRD and XPS Analyses

Figure 1 shows the XRD patterns obtained from pristine MoS_2 and Mxene/MoS_2 electrodes. Nevertheless, there are apparent variations in peak heights that correspond to the individual peaks, and fortunately both samples have good crystallinity [21]. The XRD spectrum pattern of an exfoliated pure MoS_2 electrode is shown. The data shows peaks at angles of 14.6°, 33°, 36.1°, 39.7°, 50°, and 60.6°, with corresponding d-spacing of 6.07, 2.72, 2.49, 2.27, 1.82, and 1.53Å. Minor peaks emerge at angles of 14.6, 33, 39.7, and 60.6°, which correspond to the MoS2 crystal planes (002), (101), (103), and (110), correspondingly; this is consistent with the standard reference. A reduction to a lower intensity of peak at 2θ of 32.9, 36.1, and 50° from MoS_2 patterns can be detected by observing the achieved results of peaks of data varying from pure MoS2 electrode up until MXene/MoS_2 hybrid electrode [22]. This shows the ability of MXene material to unload on the exfoliated MoS2 electrode. The lack of the Al peak around ~38° indicates the effective removal of the Al layer from the MAX phase material.

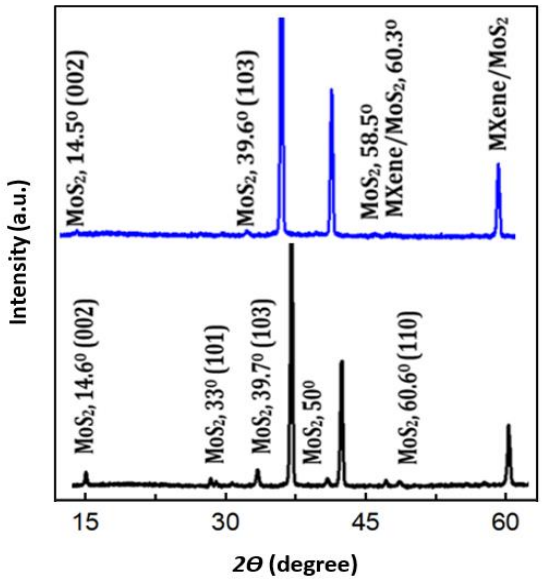

Figure 1. XRD spectra of pure MoS_2 (black) and MXene/MoS_2 electrode (blue).

MoS_2 and Ti_3C_2 MXene's surface chemical properties were evaluated using XPS; the complete spectra are displayed in Figures 2(a) and (b), respectively. The XPS graph shown in Figure 2(b) shows notable peaks that are associated with Ti 2p and C 1s, but no signal indicative of Al is found in the pure Ti_3C_2 MXene. This monitoring highlights how the HF acid treatment successfully removed the Al layers and concurrently introduced fluorine and oxygen [23]. The C 1s high-resolution spectra associated with Ti_3C_2 all arise in the relatively narrow region of 281.9–282.0 eV, regardless of the type of termination present. This prompt derives from C atoms occupy in the Ti octahedra [24]. The Ti 2p spectrum exhibits a dual-peaked structure, as shown in Figure 2(d), roughly around 455 eV and 463 eV, which correspond to Ti 2p3/2 and Ti 2p1/2, respectively. This splitting results from interactions between spin and orbit, and both peaks contain valuable information about the bonding conditions of titanium [25].

Furthermore, Figure 2 (e) confirms the formation of MoS_2 resolution XPS spectra of Mo 3d. In the Mo 3d spectrum, two prominent peaks are found at 229.5 and 232.6 eV, corresponding to the 3d5/2 and 3d3/2 states of MoS_2, respectively. Into the bargain, a peak observed at 226.7 eV can be attributed to the S 2s state of MoS_2, while another peak situated at a greater energy level, around 235.8 eV, is associated with Mo6+. This Mo6+ peak signifies a slight oxidation of the Mo edges within MoS_2, transitioning from the Mo4+ state to the Mo6+ state [26]. In addition, Figure 2 (f) shows the S 2p spectra, wherein two distinct peaks are fitted at 162.31 and 161.5 eV, correlates to the S 2p1/2 and S 2p3/2 states, respectively. These findings provide additional confirmation of the presence of MoS_2 on the MXene layers.

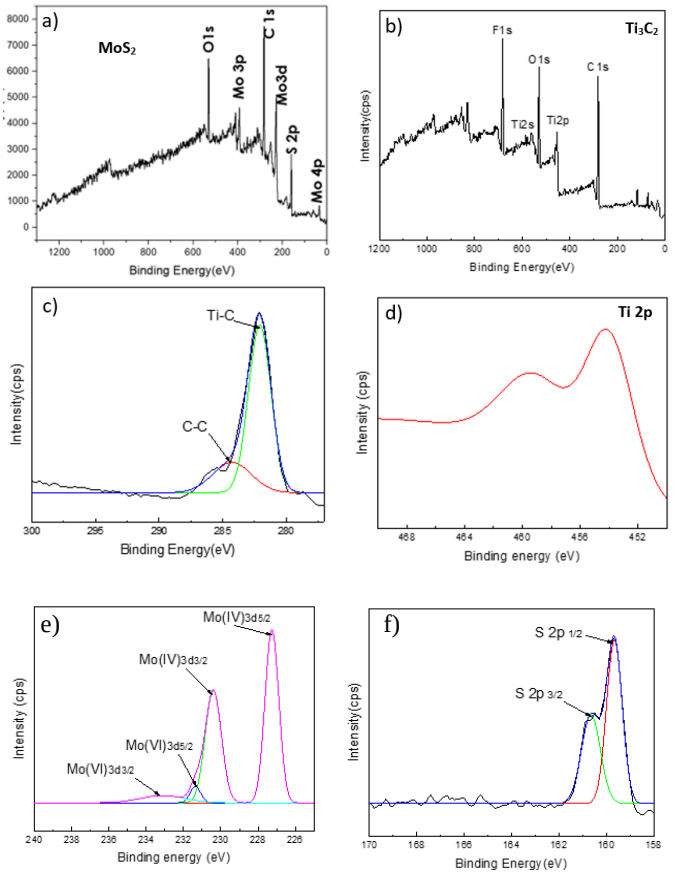

Figure 2. (a) XPS profiles of the MoS_2 samples; (b) XPS profiles of the Ti_3C_2 samples; (c) C 1s spectra of the Ti_3C_2 MXene and; (d) Ti2p spectra of Ti_3C_2 MXene; (e) Mo3d spectra of MoS_2 and; (f) S2p spectra of MoS_2.

3.2. Morphological Analysis Based on FESEM and HRTEM

The FESEM images shown in Figure 3 (a) and (b) revealed that the Ti_3C_2 MXene exhibits a layered structure, consistent with its synthesis from the selective etching of aluminium layers from Ti_3AlC_2. The layered nature is a hallmark feature of MXenes and is evident as stacked sheets or flakes [27]. The surface topography appears relatively smooth, with some observable wrinkles and undulations. These features are attributed to the inherent flexibility and mechanical properties of MXene nanosheets [28]. Figure 3 (d) and (e) depict the morphological characteristics of pure MoS_2. These samples showcase the presence of lamellar nanoflower-like MoS_2 structures. Lastly, Figure 3 (c) and (f) present images detailing the morphological features of hybrid MXene/MoS_2 structures. These images vividly illustrate the attachment of MoS_2 to the MXene, which plays an important role in effectively preventing the restacking of individual MoS_2 layers. This phenomenon enhances the utility of MXene in optimizing the structural integrity of MoS_2, a point that is critical for further comprehensive understanding [29].

HR-TEM was employed to further examine the micro-nano structures of Ti_3C_2 MXene and MoS_2, and the data are presented in Figure 4. From the TEM image of Ti_3C_2, as shown in Figure 4 (a), it is confirmed that Ti_3C_2 exhibits a layered structure following the exfoliation of Ti_3AlC_2,

aligning with previous research findings [30]. The thickness of a single layer of Ti_3C_2. Notably, the observed *d*-spacing value of the core's lattice plane was approximately 2.44 nm, which was calculated using the Gatan software, closely matching the (310) plane of TiO_2, as shown in Figure 4 (c). As XRD characterization did not provide substantial evidence of oxidation, this implies that partial oxidation of Ti_3C_2 MXene may have took place during the exfoliation process.

As shown in Figure 4 (d), the MoS_2 material, as synthesized, exists in the configuration of aggregated layers rather than in an isolated form.

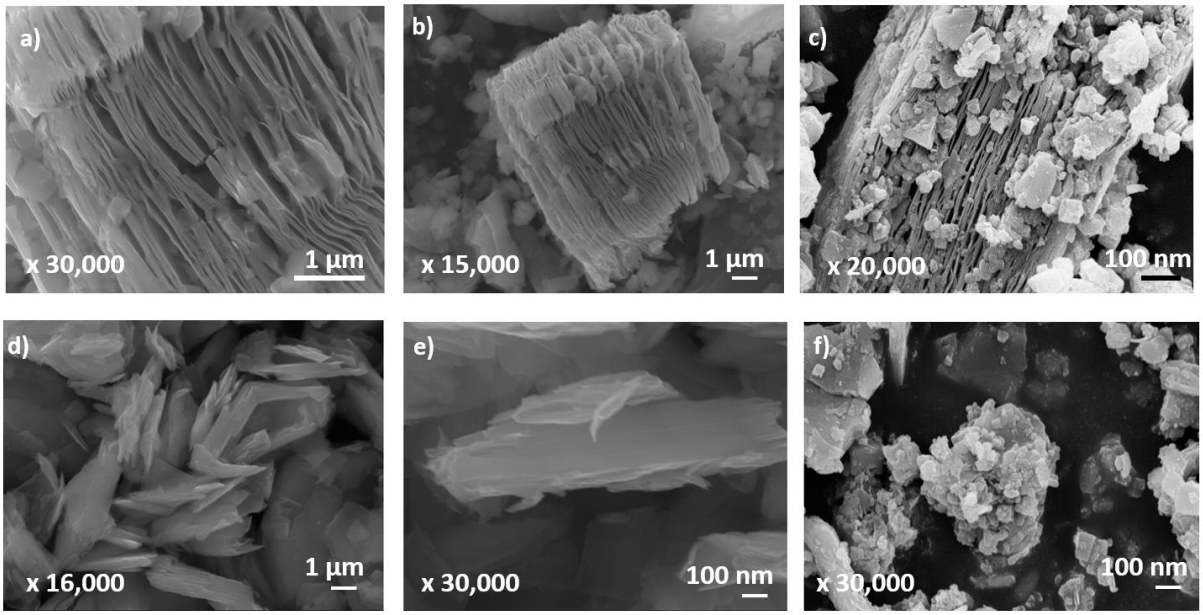

Figure 3. (a) FESEM image of Ti_3C_2 powder after HF treatment and (b) with lower magnification; (c) FESEM image of MXene/MoS_2 hybrid material; (d) FESEM image of MoS_2 powder and (e) with lower magnification; (f) MoS_2 sphere on the MXene/MoS_2 hybrid.

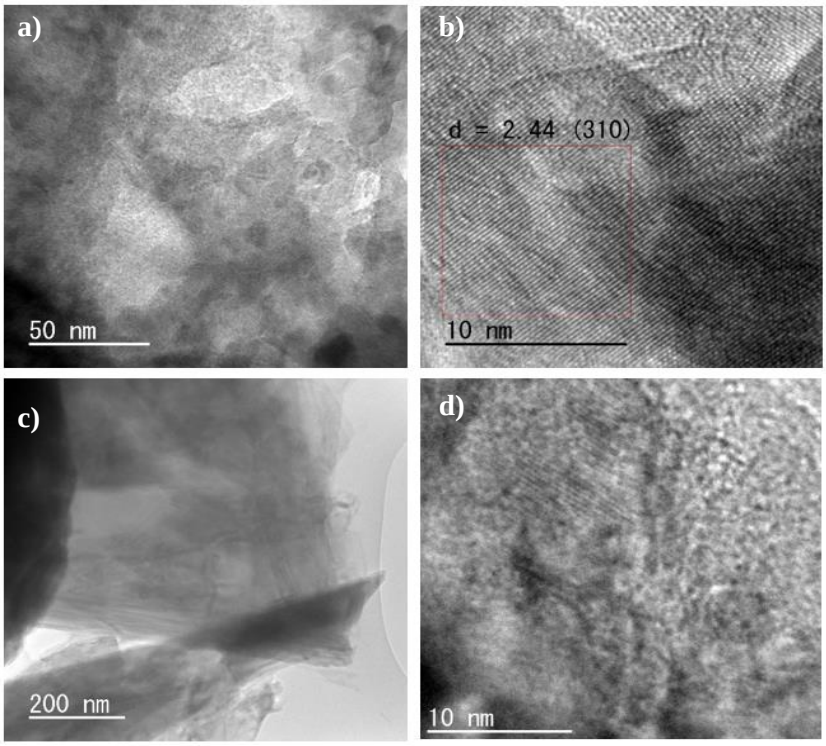

Figure 4. (a) TEM image of Ti_3C_2 after HF treatment and (b) high-resolution image (c) TEM image of MoS_2 and (d) high-resolution image.

3.3. Electrochemical Measurement

Figure 5 shows the cyclic voltammetry (CV) curves of the MXene/MoS_2 symmetrical supercapacitor at different scan rates. The calculated C_{sp} values are presented in Figure 5 and tabulated in Table 2. It is clear that there are no redox reaction peaks recorded, which indicates that the electrode exhibited good capacitive behaviour for a symmetric supercapacitor. The figure also The relatively not-so-high calculated C_{sp} value as compared to the literature data is most probably due to the high electrode loading or high active mass on the current collector [31]. Possibly, minimizing the electrode active mass might be a potential solution for achieving a high specific capacitance value. When the electrode loading is minimized, the whole or complete potential of each element inside the electrode may play a crucial role in enhancing the storage ability. Another matter to consider would be the coating technique applied during the preparation of the electrode [32]. Enhancing coating techniques in material synthesis holds significance for bolstering the future performance, durability, and functionality of coated materials.

Table 2 Specific gravimetric capacitance of MXene/MoS_2 hybrid electrode from CV analysis, calculated using (1)

Area under curves	Scan rates (mVs^{-1})	C_{sp} (Fg^{-1})
1.95 x 10^{-3}	1	139.71
3.03 x 10^{-3}	10	44.59
7.39 x 10^{-3}	50	21.74
8.52 x 10^{-3}	100	12.53
11.00 x 10^{-3}	250	6.47

The supercapacitor exhibited a quasi-rectangular-shaped curve for its CV, also confirming that this hybrid electrode shows good electrochemical double-layer capacitance (EDLC) behaviour [33]. When a lower scan rate was applied, the ion diffusion became slower; thus, the interaction between electrodes and electrolytes could be maximized. Also, the high-concentration electrolyte provides a higher number of ions, and when measured at a lower scan rate, the electrolyte ions have sufficient time to penetrate electrode pores and finally yield a better electrical charge storage for a good capacitance value [34]. Combining MXene and MoS_2 helped in increasing the active area, thus improving the charge–discharge process. Another reason for a lower C_{sp} is probably the synthesis method not involving the delamination of Ti_3C_2 and oxidation, which is known to hinder the performance of MXene. On the other hand, higher scan rates allowed more current flow and led to quick ion diffusion, during which electrolyte ions were unable to fully penetrate electrode pores but only on the surface instead [35]. In contrast, when a lower value of scan rates is applied, the capability to capture the details is more accurate; thus, it takes longer to complete testing and yield a more accurate result.

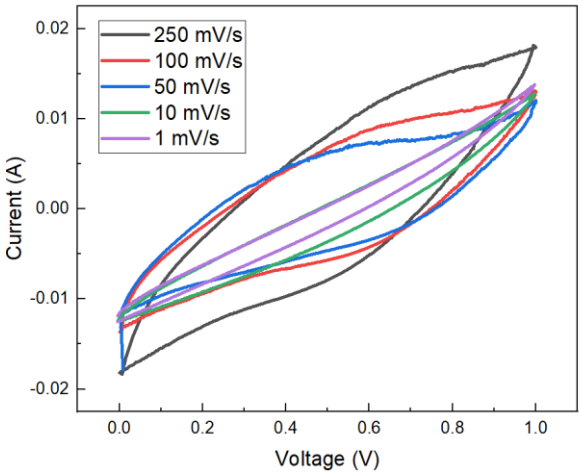

Figure 5. CV curves of the MXene/MoS_2 hybrid electrode at 1 – 250 mV/s in 6M KOH electrolyte.

The galvanostatic charge–discharge data are depicted in Figures 6 (a) and (b). The charging and discharging were found to be symmetric at around 77 secs for both charge and discharge. The unequal charge–discharge time indicated that the electrodes in such compositions are not really stabilized [36]. Furthermore, the C_{sp} values calculated using Equation (2) were very low, because of the high current applied, leading to too rapid a charge–discharge process, and this is common for symmetric supercapacitor. As referred to in Table 3, the C_{sp} values for 3.0, 6.0, 9.0, and 15.0 mA are not greater than 20 Fg^{-1}. Therefore, instead of studying the insignificant value achieved from the current density of 0.15 to 2.42 Ag^{-1}, the GCD result at 2.42 Ag^{-1} is taken for further discussion. Generally, at 15.0 mA, when a higher current density is applied, increasing the applied current causes the charge–discharge process to happen too rapidly and results in a vast time difference, which leads to very low C_{sp}.

Another possible reason for relatively low capacitance is due to the huge iR drop of approximately ±50% (up to 0.5V), as observed in the majority of the GCD curves (Figure 6). The high resistances owned by the whole supercapacitor system including electrode, electrolyte resistances caused the iR drop, and therefore, the potential value was used to compensate the resistivity. Another possible reason is the oxidation of MXene surfaces. Oxidation can introduce impurities and alter the desired properties of the material [37]. The process of oxidation can lead to the formation of additional functional groups on the electrode surface, which can enhance the electrochemical activity and improve the capacitance performance of the supercapacitor. For example, the initial oxidation of graphene-oxide precursors has been demonstrated to directly correlate with the final supercapacitor performance. It is crucial to prevent raw materials from oxidizing during the synthesis process, for example, to perform material synthesis in an inert gas environment, such as nitrogen (N_2) or argon (Ar). Nevertheless, these inert gases displace oxygen and moisture, creating a low-oxygen environment, which prevents oxidation.

Table 3 Specific capacitance of MXene/MoS_2 hybrid electrode from GCD analysis

Discharging time (sec)	Applied Current (mA)	Current Density (Ag^{-1})	Specific Capacitance (Fg^{-1})
154.96	1.0	0.15	23.24
28.10	3.0	0.48	13.49
14.10	6.0	0.96	13.54
3.60	9.0	1.61	5.80
1.90	15.0	2.42	4.56

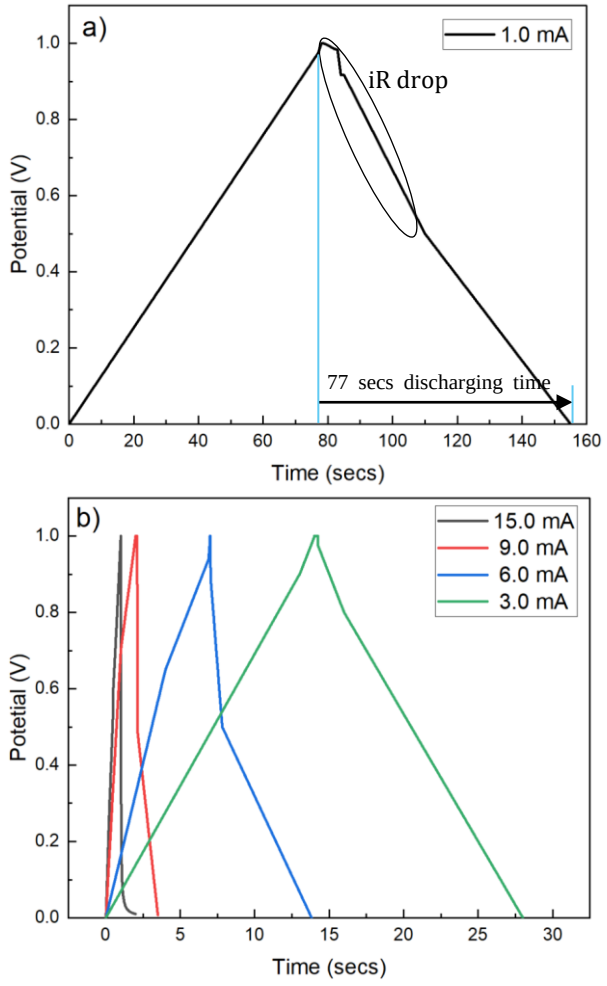

Figure 6. GCD pattern of the MXene/MoS_2 hybrid electrode for (a) 1.0 mA and (b) 3.0, 6.0, 9.0, 15.0 mA.

Recordings were taken to measure the specific capacitance of MXene/MoS_2 at regular 100-cycle intervals out of a total of 10,000 cycles, as depicted in Figure 7. Despite low C_{sp} values obtained from CV and GCD tests, a remarkable cyclic performance of the material was observed. The cyclic performance of MXene/MoS_2 was evaluated over 10,000 cycles at a current of 6.0 mA, equivalent to 0.96 Ag^{-1}, within a voltage range of 0.0–1.0 V. After 10,000 cycles, MXene/MoS_2 retained 82.58% of its initial discharge capacitance. The specific current density was chosen because it represents an optimal value for the GCD parameters, neither too high nor too low. In summary, the capacitance retention of MXene/MoS_2 after 2,000, 4,000, 6,000, and 8,000 cycles was 96.15%, 96.71%, 93.87%, and 90.75%, respectively. Measurements were also conducted at current levels of 9.0 mA and 15.0 mA over a span of 1,000 cycles to evaluate the samples' ability to maintain significant capacitance retention under high current conditions. The findings indicate that, despite a declining trend at 15.0 mA, the samples still achieved a cycle retention of 79.34% after 1,000 cycles, while at 9.0 mA, the retention was 83.34%, as shown in Figure 7. This demonstrates that the samples are capable of enduring high current levels during extensive cycle testing.

In cyclic tests for supercapacitor applications, it is common for the first 100 to 200 cycles to show instability and noise. This may be attributed to the formation of a solid electrolyte interphase (SEI) layer. During the initial charge–discharge cycles, the inauguration of an SEI layer on the electrode-electrolyte interface can cause instability and noise in the voltage profile [38].

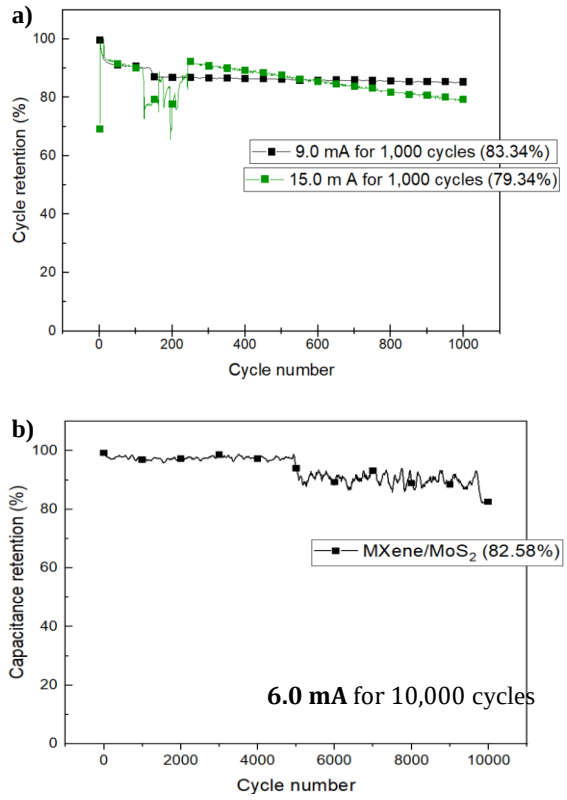

Figure 7. Cycling stability was examined at an applied current of (a) 9.0 mA for 1,000 cycles and 15.0 mA for 1,000 cycles. (b) 6.0 mA for 10,000 cycles.

After 10,000 cycles of capacitance retention testing, a thorough examination of the cell's physical and electrochemical characteristics revealed no noticeable changes [39]. It may be due to the sample's stored energy from the physical separation of charges, avoiding the chemical reactions that occur commonly in batteries during charge and discharge cycles. Chemical reactions can lead to material degradation and reduced performance over time. Figure 8 displays a FESEM picture of the sample with EDX taken both before and after the capacitance retention test. Apart from the potassium element, the EDX values following cycle retention revealed no discernible alterations. Here, the presence of potassium is attributed to the use of 6M KOH as the electrolyte.

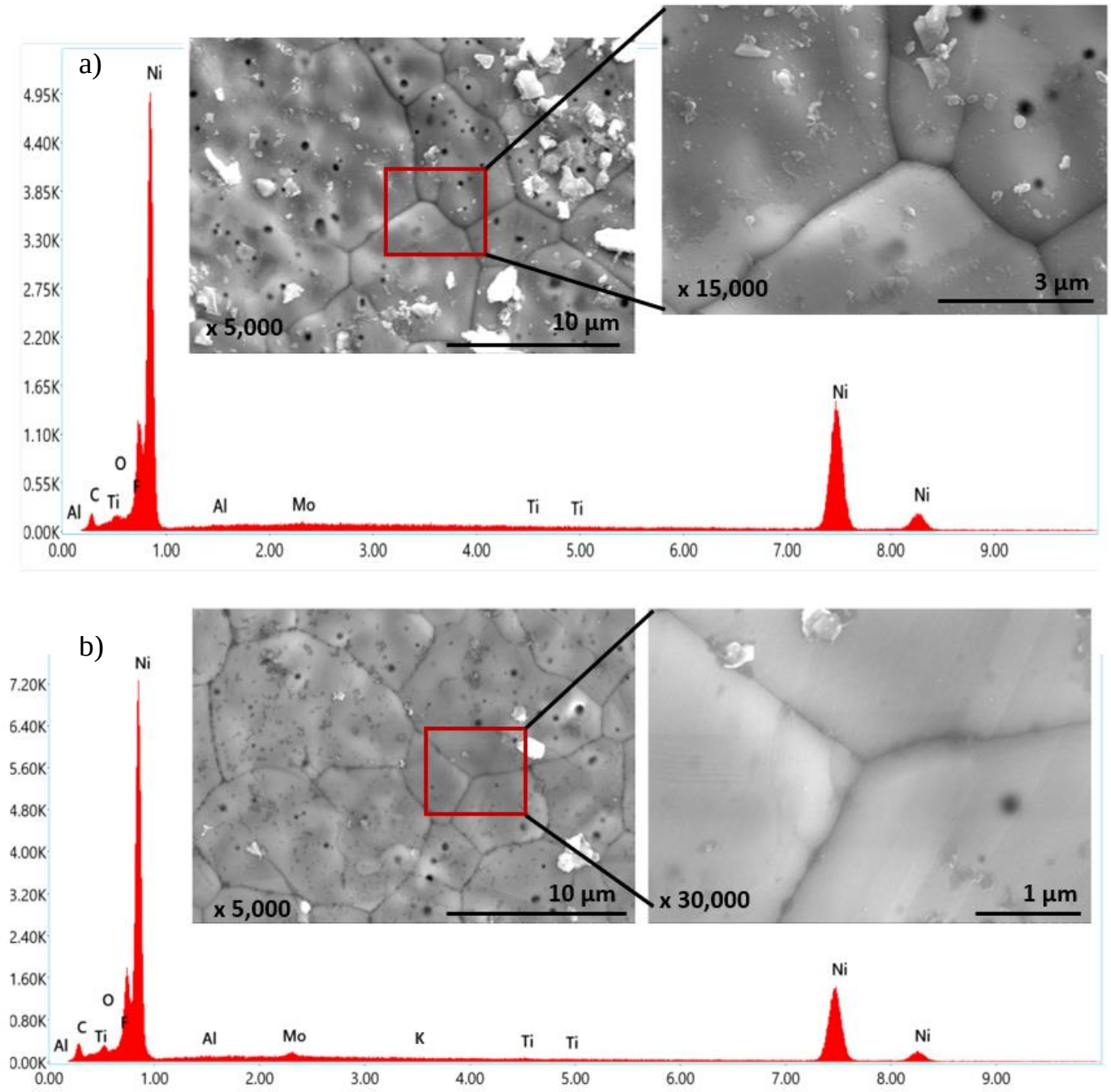

Figure 8. FESEM and EDX analyses: samples (a) before and (b) after 10,000 cycles capacitance retention evaluation.

Figure 9 shows the morphology of MXene/MoS_2 before and after 10,000 cycles. There is no significant difference, indicating that the sample can withstand high capacitance retention testing, which is good for supercapacitor applications. Further, the image indicates that the sample has retained its appearance and continues looking like a crumpled piece of paper, symbolizing the freshly crumpled sheet and structural integrity during the retention tests. However, despite those signs of long-term stability and durability, a decrease in sheets' thickness was observed, as expected [40].

The reliable and stable capacitance retention observed after an extensive testing period demonstrates the cell's strong and lasting performance, making it a great option for applications where long-term and dependable cycle retention is crucial, such as in advanced energy storage systems [41]. The images show a layered structure in line with its synthesis from Ti_3AlC_2 selectively etched aluminium layers visually, thus proving the sample's ability to withstand the harsh conditions of retention testing, which is a major consideration for the development of high-performance supercapacitors.

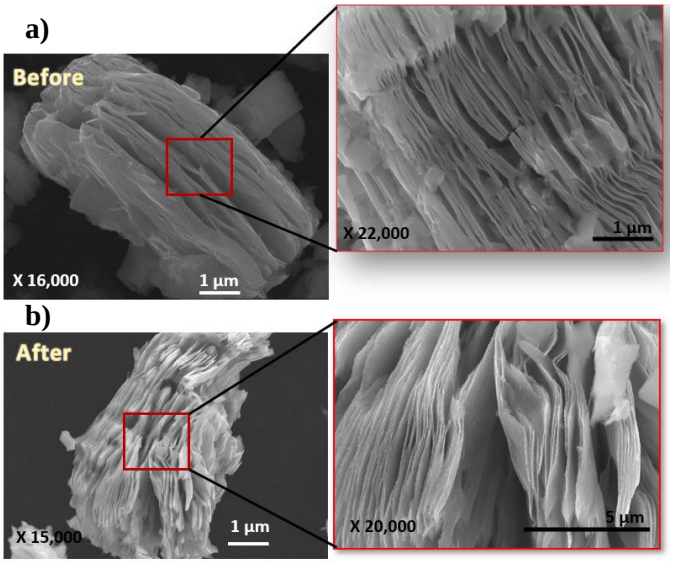

Figure 9. FESEM image of the sample (a) before and (b) after the 10,000 cycles capacitance retention measurement.

4. CONCLUSIONS

The synthesis of MXene/MoS_2 hybrid electrode was accomplished through a hydrothermal process, followed by conventional slurry coating. The XRD patterns confirmed the successful deposition of MXene Ti_3C_2 onto the exfoliated MoS_2 electrode, as well as proved that this composite heterostructure exhibits a crystalline structure. The element compositions and surface chemical states were confirmed by the XPS analysis. FESEM showed that the Ti_3C_2 MXene possesses a layered flake-like structure, aligning with its formation through the selective removal of aluminium layers from Ti_3AlC_2. Also, HR-TEM confirmed that Ti_3C_2 exhibits a layered structure following the exfoliation of Ti_3AlC_2, which is in good agreement with the literature. The electrochemical performance of the MXene/MoS_2 supercapacitor was evaluated by cyclic voltammetry (CV) and galvanostatic charge-discharge (GCD) tests, with the highest specific capacitance of 139.71 Fg^{-1}. Additionally, the device was subdue to 10,000 cycles of cyclic testing at 6.0 mA applied current, equivalent to 0.96 Ag^{-1}, with a capacitance retention of 82.58% of its initial discharge capacitance. Furthermore, even after 10,000 retention cycles, the cell remained unchanged, indicating its strong cyclic stability. Further optimization of the MXene synthesis process, specifically incorporation of the delamination step, is necessary to unlock the full potential of MXene/MoS_2 hybrid for energy storage applications.

ACKNOWLEDGMENTS

The authors are grateful to Universiti Teknikal Malaysia Melaka and Shibaura Institute of Technology, Japan for the facilities support. Special thanks to the Ministry of Higher Education for financially supporting this research under the Fundamental Research Grant Scheme (FRGS) research grant numbered FRGS/1/2021/TK0/UTEM/01/3/F00476.

REFERENCES

[1] Sun, J., Li, X., Guo, W., Zhao, M., Fan, X., Dong, Y., Chen, X., Deng, J., and Fu, Y. (2017). Synthesis methods of two-dimensional MoS_2: A brief review. Crystals, Vol. 7, issue 7, 198.

[2] Azam, M. A., Ramli, N. N. N., Mohd, N. A. N. M., Nawi, T. I. T. (2021). Recent advances in biomass-derived carbon, mesoporous materials, and transition metal nitrides as new electrode materials for supercapacitor: A short review. International Journal of Energy Research, Vol. 45, issue 6, 8335-8346.

[3] Pan, Z., Lu, Z., Xu, L., and Wang, D. (2020). A robust 2D porous carbon nanoflake cathode for high energy-power density Zn-ion hybrid supercapacitor applications. Applied Surface Science, Vol. 510, 145384.

[4] Kirubasankar, B., Narayanasamy, M., Yang, J., Han, M., Zhu, W., Su, Y., Angaiah, S., and Yan, C. (2020). Construction of heterogeneous 2D layered MoS_2/MXene nanohybrid anode material via interstratification process and its synergetic effect for asymmetric supercapacitors. Applied Surface Science, Vol. 534, 147644.

[5] Gupta, H., Chakrabarti, S., Mothkuri, S., Padya, B., Rao, T. N., and Jain, P. (2020). High performance supercapacitor based on 2D-MoS nanostructures. Materials Today: Proceedings, Vol. 26, part 1, 20–24.

[6] Kang, M. T., Thanikanti, S. B., Ramachandaramurthy, V. K., Padmanathan, K., Sunil, G. S., and Raveendran, S. K. (2021). Empowering smart grid: A comprehensive review of energy storage technology and application with renewable energy integration. Journal of Energy Storage, Vol. 39, 102591.

[7] Nikola, V., Dragan, M., Dumnić, B., and Bane, P. (2020). Comparative analysis of the supercapacitor influence on lithium battery cycle life in electric vehicle energy storage. Journal of Energy Storage, Vol. 31, 101603.

[8] Azam, M. S., Seman, R. N. A. R., Mohamed, M. A., Ani, M. H. (2022). Effect of Polytetrafluoroethylene Binder Content on Gravimetric Capacitance and Life Cycle Stability of Graphene Supercapacitor. Int. J. Automot. Mech. Eng., Vol. 19, issue 3, 9964–9970.

[9] Saravanakumar, B., Mohanty A., Suresh K. B., Kim S., and Ananthakumar, R. (2020). Comprehensive insight into the mechanism, material selection and performance evaluation of supercapatteries. Nano-Micro Letters, Vol. 12, issue 1, 85.

[10] Yang, Z., Zhu, L., Chaonan, L., Zhang, R., Wang, H., Wang, J., and Zhang, Q. (2021). Defect engineering of molybdenum disulfide for energy storage. Materials Chemistry Frontiers, Vol. 5, issue 16, 5880–5896.

[11] Kosnan, M. A., Azam, M. A., Safie, N. E., Munawar, R. F., and Takasaki, A. (2022) Recent Progress of Electrode Architecture for MXene/MoS2 Supercapacitor: Preparation Methods and Characterizations. Micromachines, Vol. 13, issue 11, 1837.

[12] Azam, M. A., Safie, N. E., Aziz, M.F. A., Seman, R. N. A. R., Suhaili, M. R. (2021). Structural characterization and electrochemical performance of nitrogen doped graphene supercapacitor electrode fabricated by hydrothermal method. International Journal of Nanoelectronics and Materials, Vol. 14, issue 2, 127-136.

[13] Rehman, J., Fan, X., Laref, A., Van, A. D., and Zheng, W. (2021). Potential anodic applications of 2D MoS_2 for K-ion batteries. Journal of Alloys and Compounds, Vol. 865, 158782.

[14] Krishnamoorthy, K., Ganesh, K. V., Radhakrishnan, S., and Kim, S. (2014). Supercapacitive properties of hydrothermally synthesized sphere like MoS_2 nanostructures. Materials Research Bulletin, Vol. 50, 499–502.

[15] Kumar, J., Prakash, P., Krithiga, T., Joshua Amarnath, D., Premkumar, J., Rajamohan, N., Vasseghian, Y., Saravanan, P., and Rajasimman, M. (2022). Methods of synthesis, characteristics, and environmental applications of MXene: A comprehensive review. Chemosphere, Vol. 286, 131607.

[16] Panda, S., Deshmukh, K., Pasha, K., Jayaraman T., Manickam, S., and Myong Y. C. (2022). MXene based emerging materials for supercapacitor applications: Recent advances, challenges, and future perspectives. Coordination Chemistry Reviews, Vol. 462, 214518.

[17] Naguib, M., Barsoum, M. W., and Yury, G. (2021). Ten years of progress in the synthesis and development of MXenes. Advanced Materials, Vol. 33, issue 39, 2103393

[18] Li, Z., Liu, Y., Li, L., Wei, Y., Caro, J., and Wang, H. (2019). Ultra-thin titanium carbide (Mxene) sheet membranes for high-efficient oil/water emulsions separation. Journal of Membrane Science, Vol. 592, 117361.

[19] Alhabeb, M., Maleski, K., Anasori, B., Lelyukh, P., Clark, L., Sin, S., and Gogotsi, Y. (2017). Guidelines for Synthesis and Processing of Two-Dimensional Titanium Carbide (Ti_3C_2Tx MXene). Chemistry of Materials, Vol. 29, issue 18, 7633-7644.

[20] Pinque, M., and Rizalinda, L. (2023). Enhanced hydrogen production through visible light photocatalysis using 2D MoS_2/2D CdS composite. World Journal of Advanced Engineering Technology and Sciences, Vol. 08, issue 1, 352–365.

[21] Xu, X., Xing, Y., and Liu, L. (2023). Construction of MoS_2-ReS2 Hybrid on Ti_3C_2Tx MXene for Enhanced Microwave Absorption. Micromachines, Vol 14, issue 11, 1996.

[22] Bashir, T., Zhou, S., Yang, S., Sara, A. I., Ali, T., Wang, H., Zhao, J., and Gao, L. (2023). Progress in 3D-MXene electrodes for lithium/sodium/potassium/magnesium/zinc/aluminum-ion batteries. Electrochemical Energy Reviews, Vol. 6, issue 1, 5.

[23] Yao, Z., Sun, H., Sui, H., and Liu, X. (2020). 2D/2D heterojunction of R-scheme Ti_3C_2 MXene/MoS_2 nanosheets for enhanced photocatalytic performance. Nanoscale Research Letters, Vol. 15, issue 1, 78.

[24] Yang, F., Ge, Y., Yin, T., Guo, J., Zhang, F., et al. (2020). Ti_3C_2Tx MXene quantum dots with enhanced stability for ultrafast photonics. ACS Applied Nano Materials, Vol. 3, issue 12, 11850–11860.

[25] Varun, N., Benchakar, M., Canaff, C., Aurélien, H., Stéphane, C., and Barsoum, M.W. (2021). A critical analysis of the X-ray photoelectron spectra of Ti_3C_2Tz MXenes. Matter, Vol. 4, issue 4, 1224–1251.

[26] Lars-Åke, N., Persson, P., and Rosén, J. (2020). X-ray photoelectron spectroscopy of Ti_3AlC_2, Ti_3C_2Tz, and TiC provides evidence for the electrostatic interaction between laminated layers in MAX-phase materials. Journal of Physical Chemistry C, Vol. 124, issue 50, 27732–27742.

[27] Kang, M., Kim, Y.-A., Yun, J.-M., Khim, D., Kim, J., Noh, Y., Kang-Jun Baeg, and Kim, D. (2014). Stable charge storing in two-dimensional MoS_2 nanoflake floating gates for multilevel organic flash memory. Nanoscale, 6, issue 21, 12315–12323.

[28] Jahan, N., Hussain, S., Huzef, U. R., Manzoor, I., Pandey, S., Habib, K., Syed, K. A., Reetika, P., and Upadhyay, C. (2021). Structural, morphological and elemental analysis of selectively etched and exfoliated Ti_3AlC_2 MAX phase. Journal of Multidisciplinary Applied Natural Science, Vol. 1, issue 1, 13–17.

[29] Luo, S., Xiang, T., Dong, J., Su, F., Ji, Y., Liu, C., and Feng, Y. (2022). A double crosslinking MXene/cellulose nanofiber layered film for improving mechanical properties and stable electromagnetic interference shielding performance. Journal of Materials Science and Technology, Vol. 129, 127–134.

[30] Li, J., Rui, B., Wei, W., Nie, P., Chang, L., Le, Z., Liu, M., Wang, H., Wang, L., and Zhang X. (2020). Nanosheets assembled layered MoS_2/MXene as high-performance anode materials for potassium ion batteries. Journal of Power Sources, Vol. 449, 227481.

[31] Najib, S., & Erdem, E. (2019). Current progress achieved in novel materials for supercapacitor electrodes: mini review. Nanoscale Advances, Vol. 1, issue 8, 2817–2827.

[32] Naguib, M., Olha, M., Lukatskaya, M. R., Dyatkin, B. L., Zhang, C., Presser V., and Barsoum, M. W. (2014). One-step synthesis of nanocrystalline transition metal oxides on thin sheets of disordered graphitic carbon by oxidation of MXenes. Chemical Communications, Vol. 50, issue 56, 7420–7423.

[33] Arunkumar, M., and Paul, A. (2017). Importance of Electrode Preparation Methodologies in Supercapacitor Applications. ACS Omega, Vol. 2, issue 11, 8039–8050.

[34] Maher, M., Hassan, S., Shoueir, K. R., Yousif, B., and Abo-Elsoud, M. A. (2021). Activated carbon electrode with promising specific capacitance based on potassium bromide redox additive electrolyte for supercapacitor application. Journal of Materials Research and Technology, Vol. 11, 1232–1244.

[35] Omid, N., Pourhosseini, S. E. M., Hamid, R. N., Francesco, D. M., and Dutta, A. (2021). Integrated hybrid architecture of metal and biochar for high performance asymmetric supercapacitors. Scientific Reports, Vol. 11, issue 1, 5387.

[36] Cho, S., Lim, J., and Seo, Y. (2022). Flexible solid supercapacitors of novel nanostructured electrodes outperform most supercapacitors. ACS Omega, Vol. 7, issue 42, 37825–37833.

[37] Artem, T., Thiede, S., Matthias, T., Nicolas, V. D., Pape, T., and Herrmann, C. (2019). Toward data-driven applications in lithium-ion battery cell manufacturing. Energy Technology, Vol. 8, issue 2, 1900136.

[38] Wu, Q., He, T., Zhang, Y., Zhang, J., Wang, Z., Liu, Y., Zhao, L., Wu, Y., and Ran, F. (2021). Cyclic stability of supercapacitors: materials, energy storage mechanism, test methods, and device. Journal of Materials Chemistry A. Materials for Energy and Sustainability, Vol. 9, issue 43, 24094–24147.

[39] Adnana, M., and Alija, M. (2014). Impact of the soil resistivity on IR drop when applying a cathodic protection system with galvanic anodes on PCCP. WIT Transactions on the Built Environment. Vol. 137, 509-517.

[40] Lei, Y., Han, D., Dong, J., Qin, L., Li, X., Zhai, D., Li, B., Wu, Y., and Kang, F. (2020). Unveiling the influence of electrode/electrolyte interface on the capacity fading for typical graphite-based potassium-ion batteries. Energy Storage Materials, Vol. 24, 319–328.

[41] Nor, A. S., Soorathep, K., Noor, W. R., and Ahmad, A. M. (2023). Electrode polymer binders for supercapacitor applications: A review. Journal of Materials Research and Technology, Vol. 23, 3470–3491